Self-Assembly of 9,10-Bis(phenylethynyl) anthracene (BPEA) Derivatives: Influence of π–π and Hydrogen Bonding Interactions on Aggregate Morphology and Self-Assembly Mechanism

Michael Lübtow,[a,b] Ingo Helmers,[c] Vladimir Stepanenko,[a] Rodrigo Q. Albuquerque,[d] Todd B. Marder,*[b] and Gustavo Fernández*[a,c]

Dedication ((optional))

Abstract: 9,10-Bis(phenylethynyl)anthracenes (BPEAs) are an important class of dyes with various applications including chemiluminescence emitters, materials for photon upconversion and for optoelectronic devices. Some of these applications require control over the packing modes of the active molecules within the active layer, which can be effected by bottom-up self-assembly. Studies aimed at controlling the molecular organization of BPEAs have primarily focused on bulk or liquid crystal materials, while in-depth investigations of BPEA-based assemblies in solution remain elusive. In this article, we report the self-assembly of two new BPEA derivatives with hydrophobic side chains, one of them featuring amide functional groups (**2**) and the other one lacking them (**1**). Comparison of the self-assembly behaviour in solution of both systems *via* spectroscopic (UV/Vis, fluorescence and NMR), microscopic (AFM) and theoretical (PM6) studies reveals the crucial role of the amide groups in controlling the self-assembly. While for both systems the formation of H-type face-to-face π-stacks is proposed, the interplay of π-stacking and H-bonding is responsible of driving the formation of 1D stacks and increasing the binding constant two-to-three orders of magnitude. Our findings show that H-bonding is a prerequisite to create ordered BPEA assemblies in solution.

Introduction

Anthracene dyes have received considerable attention for many decades due to their simplicity, synthetic accessibility as well as excellent (photo)chemical, optical and electronic properties, such as sharp absorption and emission bands, high fluorescence quantum yields and nanosecond lifetimes.[1] These properties have enabled the use of anthracene dyes as fluorescence chemosensors[2] or as active materials for optoelectronic applications.[3] An interesting feature of anthracene derivatives in this regard is their inherent ability to establish aromatic interactions in solution and in the solid state,[4] which has been exploited to control the molecular arrangement into different morphologies. For instance, various examples of anthracene-based assemblies in the crystalline[5] or liquid crystalline (LC) state,[6] in organic[7] and aqueous solutions,[8] gel materials[9] or more complex multicomponent systems[10] have been reported.

A particularly relevant class of related anthracene-based compounds are 9,10-bis(phenylethynyl)anthracenes (BPEA), which have been applied as chemiluminiscence emitters[11] due to their high emission efficiency in the visible region of the spectrum, good solubility in various solvents, and high chemical, thermal and photostability.[12] These chromophores show a strong potential as materials for optical waveguides,[13] photon upconversion by triplet-triplet annihilation,[14] and optoelectronic devices.[15] As these applications require a high degree of molecular order within the active layer, controlling the nanometer-scale organization of the dye molecules by non-covalent interactions represents a rational strategy to achieve this goal. To date, efforts towards the construction of ordered self-assembled structures based on BPEA derivatives have been focused on solid state materials,[16] gels,[17] and LCs.[18] Little is known, however, about the self-assembly pathways of BPEAs in solution and how to tailor their packing modes in a controlled fashion by exploiting non-covalent interactions.

In this paper, we provide insights into the hierarchical self-assembly in solution of BPEA derivatives by controlling the types of non-covalent interactions involved in the process. To that end, two new hydrophobic BPEA derivatives **1** and **2** that feature a comparable spatial structure but differ in the ability to form hydrogen bonds have been synthesized (Scheme 1). While the BPEA core of **1** is decorated with three alkyl chains on each side, **2** features additional benzamide groups connecting the BPEA core and the side chains. In a recent paper, our group reported that the replacement of ester by amide groups in self-assembled BODIPY dyes leads to a relatively moderate increase (15-20 fold) in the association constant due to additional hydrogen bonds.[19e] The molecular design of this work aims at increasing considerably the aggregation propensity of **2** compared to **1** by introducing not only additional hydrogen bonding but also stronger aromatic

[a] M. Lübtow, Dr. V. Stepanenko, Prof. Dr. Gustavo Fernández
Institut für Organische Chemie, Universität Würzburg Am Hubland
97074 Würzburg (Germany)

[b] Prof. Dr. Todd B. Marder,
Institut für Anorganische Chemie, Universität Würzburg
Am Hubland, 97074 Würzburg (Germany)
E-mail: todd.marder@uni-wuerzburg.de

[c] Ingo Helmers, Prof. Dr. Gustavo Fernández
Organisch-Chemisches Institut, Westfälische Wilhelms-Universität
Münster, Corrensstraße 40, 48149 Münster (Germany)
E-mail: fernandg@uni-muenster.de

[d] Dr. Rodrigo Q. Albuquerque
School of Pharmacy and Biomolecular Sciences,
Liverpool John Moores University (LJMU), Liverpool (UK)

Supporting information for this article is given via a link at the end of the document.((Please delete this text if not appropriate))

interactions, which might ultimately lead to more significant spectral changes in spectroscopic investigations.

BPEA **1** was synthesized utilizing Pd/Cu-catalyzed Sonogashira cross-coupling reactions (Scheme 1).).[19a-c] In the first step, 9,10-dibromoanthracene **3** was lithiated with *n*BuLi via lithium-halogen-exchange to give 9,10-dilithioanthracene and butyl bromide (Scheme 1).[19a] Et_2O was used as solvent and coordinating reagent to stabilize the dilithiated anthracene-species. In the next step, iodine was added to yield 9,10-diiodoanthracene **4** as yellow needles (yield: 52%).[19a] Byproducts such as the mono-iodinated derivative were separated by recrystallization from dichloromethane. In a final step, 9,10-diiodoanthracene **4** was covalently coupled to a previously reported[19d] compound (1,2,3-tris(dodecyloxy)-5-ethynylbenzene, **5** in Scheme 1) by a Pd/Cu-catalyzed Sonogashira reaction to give the target BPEA **1** as a yellow, soft solid in 93% yield.

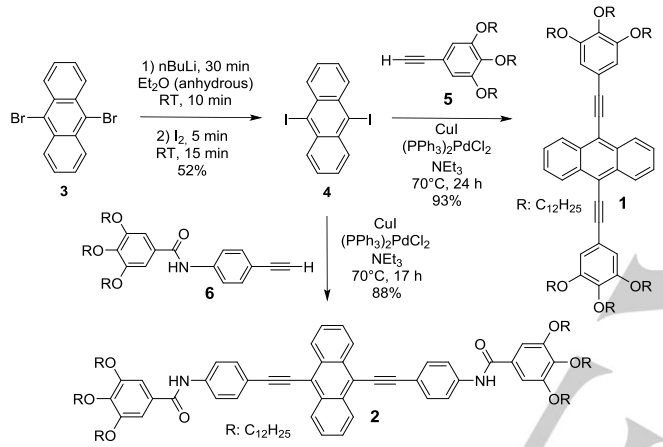

Scheme 1. Synthetic route towards BPEA **1** and **2**.

The amide-containing target BPEA **2** was synthesized using a similar procedure *via* a coupling reaction of a previously reported alkyne derivative **6**[19e] and 9,10-diiodoanthracene **4** in Et_3N at 70°C. BPEA **2** was purified by column chromatography (0%-1% THF in $CHCl_3$) and further recrystallized from a 1:4 mixture of CH_2Cl_2/hexane to give **2** as an orange, soft solid in 88% yield. All new compounds including targets **1** and **2** were characterized by ^1H and ^{13}C NMR as well as MALDI-TOF and elemental analysis (for characterization details see the Supporting Information (SI)).

Initially, solubility tests of **1** and **2** in various organic solvents were performed in order to gain information on the propensity of both systems to self-assemble. Both BPEAs are highly soluble (mM regime) in common organic solvents such as $CHCl_3$, CH_2Cl_2 and THF, suggesting a low or moderate tendency of aggregate in these media. However, significant differences are observed when moving to hydrocarbons such as toluene, hexane, cyclohexane and methylcyclohexane (MCH). While **1** shows a high solubility in these nonpolar solvents even at millimolar concentrations, more polar **2** forms turbid dispersions/solutions in these media when a concentration of ca. 0.1 mM is exceeded. As the presence of the benzamide groups is the only difference between the two systems, these results suggest an increased aggregation propensity for **2** compared to **1** due to the involvement of the aromatic amides in hydrogen bonding and π-stacking. For both molecules, we could not observe the formation of gels under the investigated conditions.

Absorption and emission studies under different conditions have been performed to gain insight into the supramolecular properties of **1** and **2**. Initially, UV/Vis-spectra in a number of solvents, including non-polar solvents as MCH and fairly polar solvents such as $CHCl_3$, were recorded. These solution spectra (1 x 10^{-5} M) display major absorption bands in the regions between 310-325 nm and 450-485 nm with vibronic fine structures, indicative of a monomeric state of **1** (Fig. 1a).[18b] The main transition at about 455 nm seems to be identical in all solvents, whereas the intensity and sharpness of the transition at ca. 475 nm is strongly solvent-dependent. For instance, in CH_2Cl_2 this transition appears well-resolved, whereas a featureless absorption band can be observed in $CHCl_3$, toluene and THF. Additionally, the bands in the region 310-325 nm remain nearly unaltered in all investigated solvents. On the other hand, for the spectrum in MCH the absorption bands at 310-325 nm and 450-485 nm are blue-shifted compared those observed in all other investigated solvents. In addition, the fact that the absorption intensity is slightly reduced in MCH points to the initial stages of a self-association process.[19e]

BPEA **2** shows comparable spectral signatures in solution (1 x 10^{-5} M) with well-resolved maxima at around 325, 455 and 485 nm in all investigated solvents (CH_2Cl_2, $CHCl_3$, THF and toluene) except MCH. For this solvent, a dramatic broadening of the absorption spectrum along with the loss of the fine vibronic structure can be observed (Figure 1b). In the UV region of the spectrum, the band at ca. 325 nm undergoes a slight blue-shift (5 nm) compared to all other solvents. Additionally, the main transition at 455 nm blue-shifts to ~430 nm and simultaneously a red-shifted shoulder at ~515 nm becomes apparent.

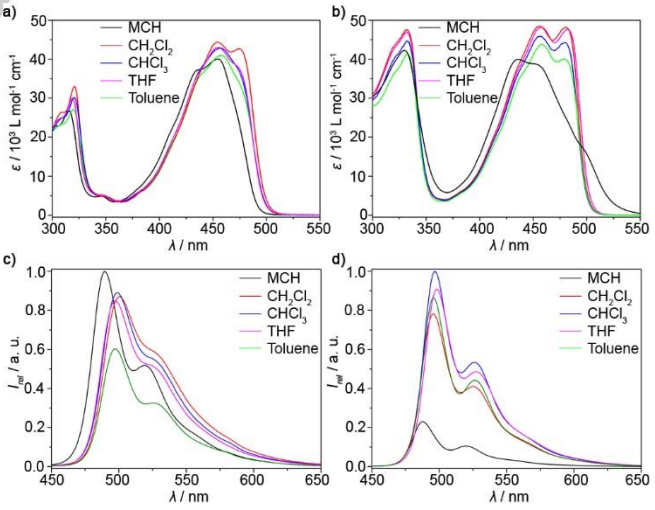

Figure 1. a,b) Solvent-dependent absorption spectra of **1** (a) and **2** (b) at room temperature (c = 1 x 10^{-5} M). c,d) Emission spectra of **1** (c) and **2** (d) in different solvents at room temperature (c = 1 x 10^{-5} M)

This spectral pattern has been previously observed for other classes of organic dyes, i.e. perylene bisimides[20] and BODIPY dyes,[19] and indicates the formation of face-to-face H-type aggregates with a twisted (rotational) dye arrangement in the stack. On the basis of these observations, BPEA **2** shows signs of aggregation in MCH, which appears to be also characteristic of hydrocarbon solvents.[19e]

To allow a comparison with UV-Vis data, **1** and **2** have been further examined by fluorescence emission studies under identical conditions using an excitation wavelength of 410 nm. The emission spectra of **1** in solution (1 x 10^{-5} M) display maxima centered at ca. 490 nm with Stokes shifts of about 40 nm (Figure 1c). A more or less pronounced second peak occurred at approximately 530 nm in all investigated solvents. It can be also observed that the emission maximum in MCH is around 8 nm blue-shifted compared to all other solvents, however the emission intensity is still quite high. In general, aggregate formation is often accompanied by fluorescence quenching, which is, however, not appreciable under diluted conditions (10^{-5} M) in any of the solvents. On the other hand, the emission properties of **2** (1 x 10^{-5} M) are nearly identical to those shown by BPEA **1** (λ_{Em} ~485 nm). The shape and position of the emission bands are almost identical in all solvents, with the exception of a dramatic quenching (ca. 80%) and a slight blue-shift (8 nm) of the fluorescence in MCH (Figure 1d). This is in agreement with the formation of H-type aggregates, as previously observed by UV-Vis spectroscopy. For both molecules, the fluorescence quantum yield in a good solvent (CH_2Cl_2) was calculated to be almost unity (0.89 for **1** and 0.98 for **2**).

Once that it has been shown that nonpolar MCH is the most promising solvent in terms of aggregation behavior, we proceeded to investigate exhaustively the self-assembly pathways of **1** and **2**. Due to the different concentration regimes at which both molecules aggregate, different spectroscopic methods were chosen. While a minimum concentration of ca. 2 mM is required for **1** to initiate self-association, amide-containing **2** was observed to readily aggregate at 1 x 10^{-5} M (Fig. 1b). Initially, concentration-dependent UV-Vis studies were performed for **1** in MCH at room temperature (r.t.). However, even at the maximum measured concentration (1 mM) using 0.01 cm cuvettes, the absorption spectrum remains nearly unchanged, revealing a lack of aggregation under these conditions. Equivalent results could be observed in temperature-dependent absorption studies in MCH, supporting the previous results (Fig. S6). A remarkably different behaviour, however, was found for **2** under similar conditions. Temperature- dependent UV/Vis-absorption studies in MCH at a concentration of 1 x 10^{-5} M reveal the occurrence of two distinct species that are stable in different temperature regimes (Fig. 2b). Between ca. 363 K and 310-315 K, only monomeric structures are present, as evident from the presence of sharp transitions at 328 nm, 450 nm and 475 nm (red spectrum in Fig. 2b). Below an approximate temperature of 310 K, the monomer units of **2** begin to self-associate, leading to a simultaneous hypsochromic shift of the absorption maximum to 433 nm and to the appearance of a red-shifted broad transition at ca. 510 nm (Fig. 2b). Simultaneously, the high-energy transition at ca. 325 nm also becomes slightly broader upon cooling. By further decreasing the temperature to 278 K, the spectrum progressively broadens and the transitions become more pronounced. As mentioned previously, these spectral signatures are in accordance with an H-type excitonic coupling of rotationally stacked BPEA dyes within the self-assembled structure.

Next, temperature-dependent fluorescent experiments were carried out in an attempt to monitor the transition completely from monomer to self-assembled species for both **1** and **2**. As the concentration required for fluorescence and UV-Vis spectroscopy lies in a similar range, it is expected that the monomer-to-aggregate transition can be fully covered at least for **2**, whereas the suitability of these studies for **1** depends on the maximum concentration that can be measured. It turned out that fluorescence experiments can be performed for **1** at a maximum concentration of 10 mM without losing resolution. Above this threshold, a dramatic decrease in signal-to-noise ratios prevent the analysis of the spectra. Thus, we selected the concentration of 10 mM for temperature-dependent studies of **1** in MCH (Fig. 2c). Initially, the sample was heated to 363 K and maintained at that temperature to ensure the formation of a molecularly dissolved state. The solution was then slowly cooled to 283 K using an identical cooling rate as in previous temperature-dependent UV/Vis studies.

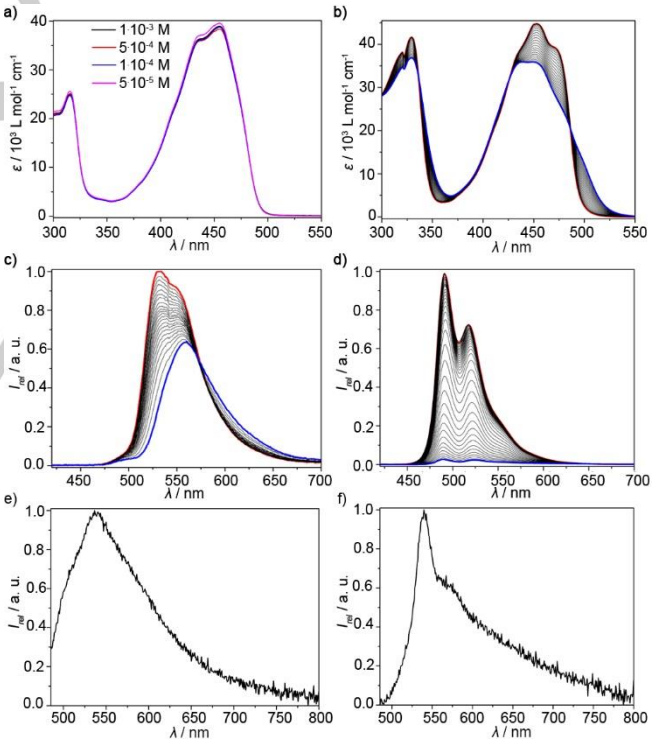

Figure 2. a) UV-Vis studies of **1** in MCH at various concentrations (298 K). b) Temperature-dependent absorption spectra of **2** (c = 1 x 10^{-5} M) between 363 K (red) und 283 K (blue spectrum). c,d) Temperature-dependent emission spectra of **1** (c) and **2** (d) in MCH between 363 K (red spectra) and 283 K (blue spectra) at a concentration of 10 mM (c) and 1 x 10^{-5} M (d). e,f) Emission spectra in thin films (from CH_2Cl_2) of **1** (e) and **2** (f).

The experiments show an initial broad emission band at ca. 532 nm that decreases in intensity in favour of a broader, red-shifted band at 559 nm (Fig. 2c). A clear isosbestic point at 573 nm can be observed, suggesting an equilibrium between two different species. The plots of emission intensity *vs* temperature extracted from these studies at various wavelengths yield a hyperbolic curve, indicating that the transition between the two species in equilibrium is not complete at 10 mM (Fig. S24). Thus, on the basis of these findings, fluorescence studies are indeed able to monitor the aggregation of **1**, but not to a sufficient extent to elucidate the self-assembly mechanism. The self-organization of **2**, on the other hand, could be monitored successfully by temperature-dependent experiments under conditions equivalent to those used for **1**. The emission spectrum of **2** in MCH at 363 K displays two emission at ca. 495 and 545 nm, consistent with the existence of a molecularly dissolved state. On cooling to 283 K, a strong fluorescence quenching and slight blue-shift of both emission bands occurs (Fig. 2d), while the shape of the spectra remains nearly unchanged. This decrease in emission is a common feature of H-type aggregates and is in line with previous UV/Vis experiments.

To compare the self-assembly with the packing of **1** and **2** in the bulk state, fluorescence spectra in thin films were recorded. To this end, samples of **1** and **2** were sheared between two glass slides to obtain thin films of both compounds. The emission spectrum of **1** in the solid state shows a comparable shape to that previously measured in solution at 10 mM and low temperature (283 K), suggesting a comparable packing in concentrated solutions and in thin films (Fig. 2e). The transition in the solid state is centered at ca. 539 nm and exhibits a fluorescence quantum yield Φ_{fl} of 9.6%. BPEA **2** shows an almost identical fluorescence quantum yield (10.8%) and position of the emission maximum (540 nm, Fig. 2f); however the maximum becomes much sharper than that of **1**, suggesting a more ordered H-type dye organisation.

The overall absorption and emission studies thus suggest that both BPEAs **1** and **2** self-assemble into H-type aggregates, but that the concentration range in which these are stable differs for the two compounds. This behaviour can be explained in terms of a reduced aggregation tendency of **1**, and therefore, a higher solubility in nonpolar solvents due to attenuated π–π interactions and the lack of possibility to form hydrogen bonds. In contrast, the polar amide groups and the largest aromatic core confer a lower solubility on **2** in nonpolar solvents and stronger intermolecular interactions driven by cooperative aromatic and hydrogen bonding interactions.[21] Whereas UV/Vis and fluorescence studies have been employed successfully to monitor fully the monomer-to-aggregate transition of **2**, the high concentration required for **1** to form a fully aggregated state cannot be covered by these studies. Thus, we decided to switch to temperature- and concentration-dependent ^{1}H NMR experiments to examine in detail the aggregation behaviour of **1**. Various concentrations between 5 and 100 mM in MCH-d_{14} were chosen for the temperature-dependent NMR studies whereas dilution studies were performed at 298 K. Both experiments display a progressive broadening and shielding of all resonances when the temperature is decreased from 363 K to 253 K or the concentration is increased (Fig. 3 and S21 and 22).

These results indicate a face-to-face π-stacking of the monomer units of **1** into aggregate species.[22] Even though that the NMR signals are still slightly shielded even at the highest concentration (100 mM) and lowest temperature (273 K), we were able to monitor the transition from monomer to aggregate upon cooling almost in its entirety.

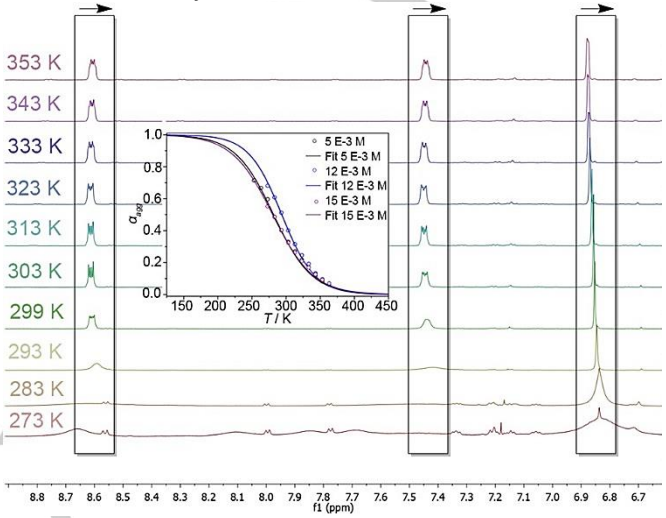

Figure 3. Temperature-dependent ^{1}H NMR studies (c = 100 mM) of **1** in MCH-d_{14} between 353 and 273 K. Inset: Plot of α_{agg} vs. T obtained by monitoring the chemical shifts (phenyl/methylene) in temperature-dependent ^{1}H NMR studies at three concentrations (1, 12 and 15 mM) and fits to the isodesmic model.

Thus, after having shown that the monomer-to-aggregate transition of both **1** and **2** can be monitored, we have inspected the thermodynamics associated with this process. To this end, the changes detected in temperature-dependent UV/Vis and fluorescence studies (for **2**) and NMR studies (for **1**) were monitored as a function of temperature. The plots of fraction of aggregated species (α_{agg}) extracted by monitoring the chemical shifts of the phenyl and methylene protons of **1** *vs* temperature yield a sigmoidal curve, which is typical of an isodesmic or stepwise self-assembly mechanism (Fig. 3, inset).[21] All plots at various concentrations show a nearly sigmoidal shape, however one can observe that the upfield shifts at a certain temperature are more pronounced at higher concentrations. For all cases and due to the fact that it was impossible to increase further the concentration due to precipitation above 150 mM, a clear plateau in the curves cannot be reached. The curves were fitted using the isodesmic model yielding values of binding constant of 37-120 M^{-1} (Table 1). This additive, non-cooperative behaviour[23] is expected considering that aromatic interactions represent the chief driving force for the self-assembly of **1** and no additional supportive interactions can occur. This situation is, however, remarkably different for **2**, which features, additionally, amide functional groups for hydrogen bonding and two additional aromatic rings. The cooperative effect of aromatic and hydrogen bonding interactions in this case is expected to direct better dye organisation than that for **1**, leading to more stable assemblies with a higher association constant. In order to examine this, the

spectral changes previously observed in temperature-dependent UV/Vis and fluorescence studies were analysed *vs.* temperature. Figure 4 depicts the plot of fraction of aggregated species (α_{agg}) *vs* temperature extracted from UV/Vis and fluorescence studies in MCH at various concentrations. In both cases, changes in the absorption or emission upon cooling a monomer solution have been monitored at 450 nm and 500 nm, respectively. A cooling rate of 1 K/min was chosen to ensure thermodynamic equilibrium although decreasing the cooling rates down to 0.2 K/min did not influence the shape of the curves. Comparable non-sigmoidal plots were extracted from both UV/Vis and fluorescence studies, indicating the reliability of the data. All curves have been successfully fitted to the cooperative nucleation-elongation model.[24] Thus, starting from a molecularly dissolved state at high temperature, **2** initially dimerises (nucleation step) when cooling to ca. 300-316 K (Fig. 4). The elongation temperatures (T_e) vary slightly depending on the concentration, between 303 and 316 K (Table 1). Further cooling below this critical temperature promotes the supramolecular polymerisation (elongation step) of **2**, which is reflected by a sharp increase in α_{agg} below the T_e. These findings are in line with a cooperative supramolecular polymerisation process.

Table 1. Thermodynamic parameters associated with the self-assembly of **1** and **2** on the basis of NMR (**1**) and combined UV/Vis and emission studies (**2**).

	C [M]	ΔG^0 [kJmol^{-1}]	ΔH^0 [kJmol^{-1}]	ΔS^0 [kJmol^{-1}K^{-1}]	T_m [K]	K [M^{-1}]
1	**5.0 ×10^{-3}**	–11.8	–24.1	0.0414	282.7 ±9.04	1.2 ×10^2
	1.2 ×10^{-2}	–10.2	–30.2	0.0671	293.7 ±4.81	60.6
	1.5 ×10^{-2}	–9.0	–22.4	0.0450	280.4 ±6.41	37.1

	C [M]	ΔH^0_{nucl} [kJmol^{-1}]	ΔH^0 [kJ mol^{-1}]	ΔS^0 [kJ mol^{-1}K^{-1}]	T_e [K]	K_{nucl} [M^{-1}]	K_{el} [M^{-1}]	σ
a	**2.0 ×10^{-5}**	–10.0 ±0.2	–51.9 ±1.1	–0.0816 ±0.0039	302.6 ±0.2	9.3 ×10^2	5.0 ×10^4	1.9 ×10^{-2}
	3.0 ×10^{-5}	–10.6 ±0.2	–48.3 ±1.0	–0.0709 ±0.0032	306.7 ±0.2	5.3 ×10^2	3.3 ×10^4	1.6 ×10^{-2}
	4.0 ×10^{-5}	–11.9 ±0.2	–40.7 ±0.9	–0.0472 ±0.0029	310.0 ±0.2	2.5 ×10^2	2.5 ×10^4	9.9 ×10^{-3}
	5.0 ×10^{-5}	–12.3 ±0.4	–42.8 ±1.6	–0.0538 ±0.0051	314.8 ±0.3	1.8 ×10^2	2.0 ×10^4	9.2 ×10^{-3}
b	**2.0 ×10^{-5}**	–3.8 ±0.9	–88.4 ±8.0	–0.2374 ±0.0275	300.7 ±0.8	1.1 ×10^3	5.0 ×10^4	2.1 ×10^{-2}
	3.0 ×10^{-5}	–5.6 ±0.4	–87.8 ±3.9	–0.1965 ±0.0130	310.2 ±0.5	3.7 ×10^3	3.3 ×10^4	1.1 ×10^{-1}
	4.0 ×10^{-5}	–9.0 ±0.6	–70.7 ± 3.8	–0.1405 ±0.0123	314.7 ±0.5	8.1 ×10^2	2.5 ×10^4	3.2 ×10^{-2}
	5.0 ×10^{-5}	–9.3 ±0.4	–71.1 ±2.5	–0.1436 ±0.0081	316.9 ±0.3	5.0 ×10^2	1.7 ×10^4	3.0 ×10^{-2}

Table 1 depicts the thermodynamic parameters associated with this process extracted from two independent (UV/Vis and fluorescence) methods. Both studies yield comparable data, with values of the degree of cooperativity (σ) between ~0.01 and 0.1, revealing a relatively low, yet appreciable degree of cooperativity. The nucleation (K_n) and elongation constants (K_e) were determined to lie in the range 2-10 x 10^2 M^{-1} and 2-5 x 10^4 M^{-1}, respectively (Table 1). Even though that most thermodynamic parameters extracted from both methods are comparable, we observed a slight discrepancy in the average K_n values (472 M^{-1} *vs.* 1345 M^{-1}) and average T_e (308.5 K *vs.* 310.6 K) obtained by both methods. This may be explained in terms of a non-linear relation between the fluorescence intensity and α_{agg}. It is likely that the first dimerization event quenches the fluorescence to a higher extent than subsequent monomer addition, possibly contributing to overestimate the emission decrease at initial stages of the aggregation process, thereby leading to a smoothening in the slope and to slightly different values of T_e and K_n.

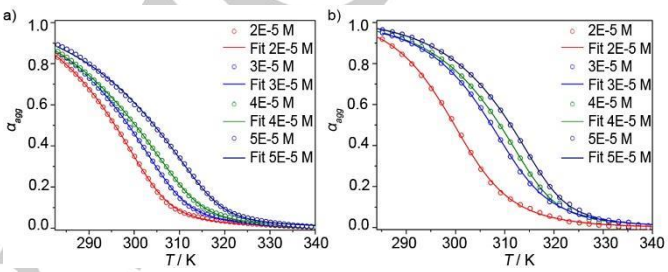

Figure 4. Cooling curves obtained by monitoring the absorption at 500 nm (a) and emission at 550 nm (b) of **2** *vs* temperature at different concentrations (2-5 x 10^{-5} M). The curves were obtained by cooling (1 K/min) a monomer solution from 343 K to 278 K. The solid lines represent the fit of the curves to the nucleation-elongation model,[24] from which the parameter α_{agg} was derived.

Thus, thermodynamic analysis of the self-assembly of **1** and **2** reveals that the sole presence of a large aromatic surface (BPEA) does not suffice to create ordered assemblies and that cooperative directional hydrogen bonds are needed to elongate the supramolecular stacks. This reasoning is logical if we consider that the elongation constant (K_{el}) of **2** is two to three orders of magnitude higher than the association constant (K) of **1**. This difference in association constant is considerably higher than that recently observed in related BODIPY dyes that only differ in the presence of ester or amide groups as linkers.[19e] For these systems, the binding constant increases around 20 times when the ester groups are replaced by amide moieties due to the introduction of additional hydrogen bonding. For our current BPEAs **1** and **2**, this difference is considerably higher (around 200-400 times) as a result of stronger π-interactions involving the larger aromatic surface of **2** along with hydrogen bonding.

To determine whether this different self-assembly behaviour would indeed lead to distinct aggregate morphologies, we investigated both BPEAs by atomic force microscopy (AFM). For that, we first prepared aggregate solutions of **1** (32 mM) and **2** (5 x 10^{-5} M) and subsequently spin-coated them on highly-oriented pyrolytic graphite (HOPG) at 7000 rpm. AFM images were then recorded. Due to the very high concentration used for **1**, only highly agglomerated material could be distinguished on HOPG. We then diluted the sample ca. five times (*c*~7 mM), thus enabling the visualisation of entangled short rod-like and/or nearly spherical aggregates with lengths up to ca. 15 nm and a relatively

uniform diameter of 3.2-3.8 nm (Fig. 5a). These dimensions are slightly shorter (ca. 0.5-1.1 nm) than the molecular length of **1** assuming a fully outstretched conformation of the alkoxy chains (4.3 nm), which implies a strong alkyl-alkyl interdigitation. Assuming a π–π stacking distance of 0.34 nm,[25] the stacks of **1** comprise a maximum number of 44 molecules. This relatively weak aggregation propensity is in agreement with a non-cooperative self-assembly process wherein monomer addition does not become more favourable upon increasing aggregate size.

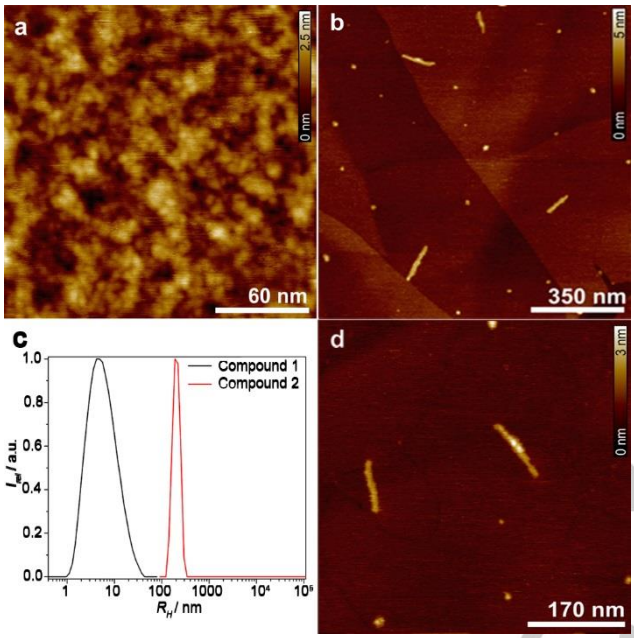

Figure 5. AFM images recorded upon spin-coating aggregate solutions of **1** (a) and **2** (b,d) in MCH onto HOPG. Concentration: ca 7 mM (a) and 5 x 10^{-5} M (b,d). c) Dynamic light scattering CONTIN plots of **1** and **2** in MCH at 30 mM and 0.1 mM, respectively (both measurements were performed at r.t.)

On the other hand, **2** self-associates into distinct aggregate morphologies on HOPG (Fig. 5b). As expected, the cooperative interplay between π–π and hydrogen bonding interactions in **2** represents a much stronger driving force than π–π interactions in isolation (as it was the case for **1**) to enable the formation of anisotropic supramolecular structures. This is evidenced by the appearance of relatively rigid (uniform width of 3.9±0.2 nm) and considerably longer (up to 190 nm in length) rod-like associates when **2** was investigated by AFM (Fig. 5b). These H-type stacks feature a maximum number of ca. 560 monomer units, which are more than 10 times longer than the rod-like aggregates formed by **1**. Similarly to **1**, the width of the rods is smaller than the molecular length of **2** (6.3 nm measured by PM6 calculations), suggesting a strong coiling of the hydrocarbon chains on the HOPG surface.
Dynamic light scattering (DLS) studies of **1** and **2** in MCH further support this trend. CONTIN analysis of the autocorrelation function of **1** shows a relatively broad size-distribution of between 1 and ca. 40 nm with a maximum at 8 nm (Fig. 5c), in good agreement with the AFM images. On the other hand, **2** forms considerably larger associates due to the cooperative effect of π–π stacking and hydrogen bonding, yielding self-assembled structures with a size distribution ranging from ca. 100 to 300 nm (Fig. 3c).

The dispersion-corrected semiempirical PM6 model in vacuum[26] was used to obtain additional insight into the aggregation patterns of **1** and **2**, as it has been used successfully to describe other similar supramolecular systems.[27,28] The optimised structures of octamers of **1** and **2** having short methoxy groups as side chains are shown in Fig. 6, in which hydrogens were omitted for clarity. The angle θ between the line joining the centre of mass of adjacent anthracenes and the long axis of one of them was about 75°, i.e., larger than the threshold value of 54.7º necessary to be considered H-aggregates,[29] which is in agreement with the photophysical data shown in Fig. 2. The respective ΔH_f values for the monomer addition were in all cases exothermic and roughly constant for **1** or slightly more negative upon growth in the case of **2** (Table S3), which reinforces the fact that the former might grow in an isodesmic fashion and the latter cooperatively. The monomer units of **1** inside the optimised stack (Fig. 6) are considerably more distorted at the edges, which is related to the lack of the long dodecyl side chains, as already discussed in our previous work.[28] Additionally, **1** is also able to form a small self-terminating seed (ΔH_f = -103.44 kJ/mol, Fig. S31) which cannot grow further due to geometrical constraints. This seed is about 14 kJ/mol less stable than the dimer used to grow the octamer shown in Fig. 6. Such dimer seeds may further aggregate in a disorganised way or even lead to the termination of the aggregate growth, which may help to explain the existence of low-ordered/short aggregates of **1** found from AFM measurements (Fig. 5a).

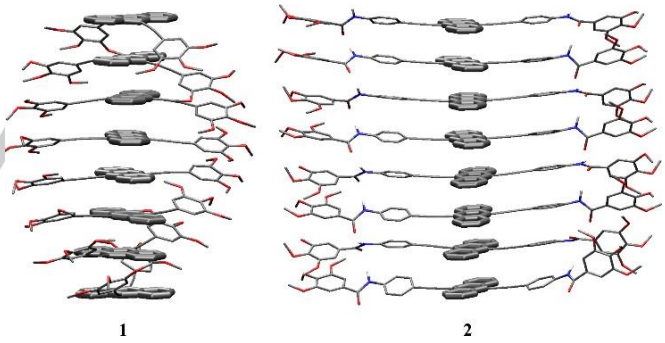

Figure 6. Geometries of octamers of **1** and **2** optimised with the dispersion-corrected PM6 model in vacuum. Non-polar hydrogens are omitted for clarity.

Interestingly, the hydrogen bonds exhibited by **2** (Fig. 6) are in a zig-zag arrangement, which is not as stabilising as the traditional linear ones. This could explain the fact that longer aggregates of **2** (length > 200 nm) were not observed experimentally by various e.g. DLS and AFM techniques. The fact that the nitrogen is directly bound to the extended π core instead of the carbonyl group increases the co-planarity of the amide and the core,[30] which hampers the formation of linear hydrogen bonds, as well as increases intra-columnar disorder.[31] Even though cooperative π–π and hydrogen bonding interactions occur in the aggregate structure, the proposed alternated arrangement

of hydrogen bonds might help rationalise the relatively moderate-to-low degree of cooperativity observed experimentally by UV/vis and fluorescence spectroscopy.

Conclusions

The aim of this work was to gain new insights into the self-assembly in solution of BPEA derivatives, a class of dyes that has been extensively exploited as active materials for optoelectronic applications. Recent reports illustrate that these dyes have a strong propensity to self-assemble into gel materials or in the solid and LC states, while details of their hierarchical supramolecular polymerization have remained elusive thus far. To tackle this subject, we have synthesized and investigated two new self-associating BPEAs (**1** and **2**) decorated with peripheral dodecyloxy chains that differ in their propensity to π-stack as well as in their ability to form hydrogen bonds. While BPEA **1** is expected to self-associate primarily by π–π interactions, its homologue **2** features additionally aromatic amide groups that can enhance the aggregation propensity by hydrogen bonding reinforced by stronger π-stacking of the larger aromatic surface. A collection of experimental (UV/Vis, fluorescence, NMR, DLS, AFM) and theoretical methods (PM6), along with thermodynamic analysis of the self-assembly of both BPEAs reveal the following results: 1) the aromatic surface of BPEA on its own does not suffice to drive the formation of anisotropic aggregates through π–π interactions; 2) cooperative hydrogen bonding forces are required in order to enable a preferential growth into supramolecular polymers; 3) the attachment of functional groups that can participate in H-bonding to the BPEA is necessary in order to switch the self-assembly mechanism from isodesmic to cooperative; 4) the association (elongation) constant increases two to three orders of magnitude when benzamide groups are introduced due to cooperative hydrogen bonds and increased π-stacking of the BPEAs. Our results provide some guidelines for the construction of organised BPEA dye aggregates which can be extended to other classes of organic dyes.

Acknowledgements

We thank the Alexander von Humboldt Foundation (Sofja Kovalevskaja) for financial support.

Keywords: Phenylethynylanthracenes • self-assembly • fluorescent dyes • cooperativity • non-covalent interactions

[1] M. Yoshizawa, J. K. Klosterman, *Chem. Soc. Rev.* **2014**, *43*, 1885-1898.

[2] L. Fabrizzi, A. Poggi, *Chem. Soc. Rev*. **1995**, 24, 197-202.

[3] a) L. Jiang, J. Gao, Y. Fu, H. Dong, H. Zhao, H. Li, Q. Tang, K. Chen, W. Hu, *Nanoscale* **2010**, *2*, 2652-2656; b) J.-P. Hong, M.-C. Um, S.-R. Nam, J.-I. Hong, S. Lee, *Chem. Commun.* **2009**, 310-312; c) J. N. Moorthy, P. Venkatakrishnan, P. Natarajan, D.-F. Huang, T. J. Chow, *J. Am. Chem. Soc.* **2008**, *130*, 17320–17333.

[4] a) S. Ehrlich, J. Moellmann, S. Grimme, *Acc. Chem. Res*. **2013**, *46*, 916-926; b) S. E. Wheeler, *Acc. Chem. Res*. **2013**, *46*, 1029-1038; c) J. W. G. Bloom, S. E. Wheeler, *Angew. Chem. Int. Ed*. **2011**, *50*, 7847-7849; d) C. A. Hunter, *Chem. Soc. Rev.* **1994**, *23*, 101-109.

[5] a) T. Kusukawa, K. Matsumoto, H. Nakamura, W. Iizuka, K. Toyama, S. Takeshita, *Org. Biomol. Chem*. **2013**, *11*, 3692–3698; b) K. Kobayashi, H. Masu, A. Shuto, K. Yamaguchi, *Chem. Mater.* **2005**, *17*, 6666-6673; c) M. J. Krische, J.-M. Lehn, N. Kyritsakas, J. Fischer, E. K. Wegelius, K. Rissanen, *Tetrahedron* **2000**, *56*, 6701-6706; d) K. Endo, T. Ezuhara, M. Koyanagi, H. Masuda, Y. Aoyama, *J. Am. Chem. Soc*. **1997**, *119*, 499-505.

[6] a) J. Luo, H. Qu, J. Yin, X. Zhang, K.-W. Huang, C. Chi, *J. Mater. Chem*. **2009**, *19*, 8202-8211; b) Y. Takaguchi, T. Tajima, Y. Yanagimoto, S. Tsuboi, K. Ohta, J. Motoyoshiya, H. Aoyama, *Org. Lett*. **2003**, *5*, 1677-1679; c) T. Kato, T. Kutsuna, K. Yabuuchi, N. Mizoshita, *Langmuir* **2002**, *18*, 7086-7088.

[7] a) D. D Prabhu, K. Aratsu, M. Yamauchi, X. Lin, B. Adhikari, S. Yagai, *Polym. J.* **2016**, doi:10.1038/pj.2016.94; b) Y. Ando, T. Sugihara, K. Kimura, A. Tsuda, *Chem. Commun*. **2011**, *47*, 11748–11750; c) M. Ikegami, I. Ohshiro, T. Arai, *Chem. Commun*. **2003**, 1566–1567.

[8] a) S. P. Patil, B. A. Moosa, S. Alsaiari, K. Alamoudi, A. Alshamsan, A. AlMalik, K. Adil, M. Eddaoudi, N. M. Khashab, *Chem. Eur. J.* **2016**, *22*, 13789-13793; b) P. Malakar, D. Modak, E. Prasad, *Chem. Commun*. **2016**, *52*, 4309-4312; c) C. Niu, Y. You, L. Zhao, D. He, N. Na, J. Ouyang, *Chem. Eur. J.* **2015**, *21*, 13983-13990; d) K. Hagiwara, M. Otsuki, M. Akita, M. Yoshizawa, *Chem. Commun.* **2015**, *51*, 10451-10454; e) Y.-X. Wang, Y.-M. Zhang, Y. Liu, *J. Am. Chem. Soc.* **2015**, *137*, 4543−4549; f) Y. Sagara, T. Komatsu, T. Terai, T. Ueno, K. Hanaoka, T. Kato, T. Nagano, *Chem. Eur. J.* **2014**, *20*, 10397-10403; g) J. Hu, P. Wang, Y. Lin, J. Zhang, M. Smith, P. J. Pellechia, S. Yang, B. Song, Q. Wang, *Chem. Eur. J.* **2014**, *20*, 7603-7607; h) A. Suzuki, K. Kondo, M. Akita, M. Yoshizawa, *Angew. Chem. Int. Ed.* **2013**, *52*, 8120-8123; i) M. Supur, Y. M. Sung, D. Kim, S. Fukuzumi, *J. Phys. Chem. C* **2013**, *117*, 12438−12445; j) Y. Liu, K. Liu, Z. Wang, X. Zhang, *Chem. Eur. J.* **2011**, *17*, 9930-9935; k) R. Iwaura, M. Ohnishi-Kameyama, T. Iizawa, *Chem. Eur. J.* **2009**, *15*, 3729-3735.

[9] a) J. Wei, Q. Chai, L. He, B. Bai, H. Wang, M. Li, *Tetrahedron* **2016**, *72*, 3073-3076; b) H. Jintoku, M.-T. Kao, A. Del Guerzo, Y. Yoshigashima, T. Masunaga, M. Takafuji, H. Ihara, *J. Mater. Chem. C* **2015**, *3*, 5970-5975; c) P. Wang, J. Hu, S. Yang, B. Song, Q. Wang, *Chem. Asian J.* **2014**, *9*, 2880-2884; d) S. K. Samanta, S. Bhattacharya, *Chem. Eur. J.* **2012**, *18*, 15875-15885; e) L. Chen, S. Revel, K. Morris, D. J. Adams, *Chem. Commun.* **2010**, *46*, 4267-4269; f) J.-P. Desvergne, A. Del Guerzo, H. Bouas-Laurent, C. Belin, J. Reichwagen, H. Hopf, *Pure Appl. Chem.* **2006**, *78*, 707-719; g) A. Del Guerzo, A. G. L. Olive, J. Reichwagen, H. Hopf, J.-P. Desvergne, *J. Am. Chem. Soc.* **2005**, *127*, 17984-17985; h) I. O. Shklyarevskiy, P. Jonkheijm, P. C. M. Christianen, A. P. H. J. Schenning, A. Del Guerzo, J.-P. Desvergne, E. W. Meijer, J. C. Maan, *Langmuir* **2005**, *21*, 2108-2112; i) T. Nakashima, N. Kimizuka, *Adv. Mater.* **2002**, *14*, 1113-1116.

[10] a) H. Zhao, S. Sen, T. Udayabhaskararao, M. Sawczyk, K. Kučanda, D. Manna, P. K. Kundu, J.-W. Lee, P. Král, R. Klajn, *Nat. Nanotech.* **2016**, *11*, 82-88; b) S. S. Babu, M. J. Hollamby, J. Aimi, H. Ozawa, A. Saeki, S. Seki, K. Kobayashi, K. Hagiwara, M. Yoshizawa, H. Möhwald, T. Nakanishi, *Nat. Commun.* **2013**, *4*, 1969; c) N. Na, X. Mu, Q. Liu, J. Wen, F. Wang, J. Ouyang, *Chem. Commun.* **2013**, *49*, 10076-10078; d) Z. Su, B. Yu, X. Jiang, J. Yin, *Macromolecules* **2013**, *46*, 3699-3707; e) M. Takahashi, N. Nishizawa, S. Ohno, M. Kakita, N. Fujita, M. Yamashita, T. Sengoku, H. Yoda, *Tetrahedron* **2009**, *65*, 2669-2677.

[11] a) M. Levitus, M. A. Garcia-Garibay, *J. Phys. Chem. A* **2000**, *104*, 8632-8637; b) B. Li, W. Miao, L. Cheng, *Dyes and Pigments* **1999**, *43*, 161-165.

[12] a) A. Demeter, *J. Phys. Chem. A* **2014**, *118*, 9985-9993; b) M. Mitsui, Y. Kawano, R. Takahashi, H. Fukui, *RSC Adv.* **2012**, *2*, 9921-9931.

[13] Y. S. Zhao, J. Xu, A. Peng, H. Fu, Y. Ma, L. Jiang, J. Yao, *Angew. Chem. Int. Ed.* **2008**, *47*, 7301-7305

[14] a) N. Kimizuka, N. Yanai, M.-a. Morikawa, *Macromolecules* **2016**, ASAP; b) N. Yanai. N. Kimizuka, *Chem. Commun*. **2016**, *52*, 5354-5370; c) T.; A. Monguzzi, F. Riva, R. Tubino, F. Meinardi, *Chem. Phys. Lett*. **2012**, *521*, 17-19; d) A. Monguzzi, R. Tubino, S: Hoseinkhani, M. Campione, F. Meinardi, *Phys. Chem. Chem. Phys. A* **2012**, *14*, 4322-4332. e) N. Singh-Rachford, F. N. Castellano, *Coord. Chem. Rev*. **2010**, *254*, 2560-2573.

[15] a) J.-Y. Wang, H.-D. Peng, J.-M. Yang, J.-H. Yan, G.-B. Pan, *Phys. Chem. Chem. Phys.* **2016**, *18*, 10836-10839; b) J. A Hur, S. Y. Bae, K. H. Kim, T. W. Lee, M. J. Cho, D. H. Choi, *Org. Lett.* **2011**, *13*, 1948-1951; c) L. Valentini, D. Bagnis, A. Marrocchi, M. Seri, A. Taticchi, J. M. Kenny, *Chem. Mater.* **2008**, *20*, 32-34; d) S. W. Cha, S.-H. Choi, K. Kim, J.-I. Jin, *J. Mater. Chem*. **2003**, *13*, 1900-1904.

[16] a) Y. Sagara, Y. C. Simon, N. Tamaoki, C. Weder, *Chem. Commun*. **2016**, *52*, 5694-5697; b) Y. Sagara, C. Weder, N. Tamaoki, *RSC Adv.* **2016**, *6*, 80408-80414.

[17] M.-T. Kao, C. Schäfer, G. Raffy, A. Del Guerzo, *Photochem. Photobiol. Sci.* **2012**, *11*, 1730-1736..

[18] a) J. Zhu, K. Zhong, Y. Liang, Z. Wang, T. Chen, L. Y. Jin, *Tetrahedron* **2014**, *70*, 1230-1235; b) S. Yamane, Y. Sagara, T. Kato, *Chem. Commun.* **2013**, *49*, 3839-3841; c) Y. Sagara, T. Kato, *Angew. Chem. Int. Ed*. **2011**, *50,* 9128-9132; d) Y. Sagara, S. Yamane, T. Mutai, K. Araki, T. Kato, *Adv. Funct. Mater*. **2009**, *19*, 1869-1875; e) R. Gimenez, M. Piñol, J. L. Serrano, *Chem. Mater*. **2004**, *16*, 1377-1383.

[19] a) P. Nguyen, S. Todd, D. Ven den Biggelaar, N. J. Taylor, T. B. Marder, F. Wittmann, R. H. Friend, *Synlett* **1994**, 299-201; b) T. M. Fasina, J. C. Collings, D. P. Lydon, D. Albesa-Jove, A. S. Batsanov, J. A. K. Howard, P. Nguyen, M. Bruce, A. J. Scott, W. Clegg, S. W. Watt, C. Viney, T. B. Marder, *J. Mater. Chem.* **2004**, *14*, 2395-2404; c) T. M. Fasina, J. C. Collings, J. M. Burke, A. S. Batsanov, R. M. Ward, D. Albesa-Jové, L. Porrès, A. Beeby, J. A. K. Howard, A. J. Scott, W. Clegg, S. W. Watt, C. Viney, T. B. Marder, *J. Mater. Chem.* **2005**, *15*, 690-697; d) J. Guilleme, J. Aragó, E. Orti, E. Cavero, T. Sierra, J. Ortega, C. L. Folcia, J. Etxebarria, D. González-Rodriguez, T. Torres, *J. Mater. Chem. C* **2015**, *3*, 985-989; e) A. Rödle, B. Ritschel, C. Mück-Lichtenfeld, V. Stepanenko, G. Fernández, *Chem. Eur. J.* **2016**, *22*, 15772-15777.

[20] a) X.-Q. Li, V. Stepanenko, Z. Chen, P. Prins, L. D. A. Siebbeles, F. Würthner, *Chem. Commun.* **2006**, 3871-3873; b) F. Würthner, B. Hanke, M. Lysetska, G. Lambright, G. S. Harms, *Org. Lett.* **2005**, 7, 967–970.

[21] a) C. Rest, R. Kandanelli, G. Fernandez, *Chem. Soc. Rev*. 2015, ***44***, 2543-2572; b) C. Kulkarni, S. Balasubramanian, S. J. George, *ChemPhysChem* **2013**, *14*, 661-673; c) T. F. A. de Greef, M. M. J. Smulders, M. Wolffs, A. P. H. J. Schenning, R. P. Sijbesma, E. W. Meijer, *Chem. Rev.* **2009**, *109*, 5687-5754.

[22] G. Fernandez, F. Garcia, L. Sanchez, *Chem. Commun.* **2008**, 6567-6569

[23] L. Tebben, C. Mück-Lichtenfeld, S. Grimme, G. Fernandez, A. Studer, *Chem. Eur. J.* **2016**, DOI: *chem.201604651*.

[24] a) H. M. M. ten Eikelder, A. J. Markvoort, T. F. A. de Greef, P. A. J. Hilbers, *J. Phys. Chem. B*, **2012**, *116*, 5291-5301; b) A. J. Markvoort, H. M. M. ten Eikelder, P. A. J. Hilbers, T. F. A. de Greef, E.W. Meijer, *Nat. Commun.* **2011**, *2*, 509-517.

[25] C. A. Hunter, J. K. M. Sanders, J. Am. Chem. Soc. **1990**, *112*, 5525-5534.

[26] J. Řezáč, P. Hobza, *J. Chem. Theory Comput*. **2012**, *8*, 141-151.

[27] N. A. M. S. Caturello, Z. Csók, G. Fernández, R. Q. Albuquerque, *Chem. Eur. J*. **2016**, *22*, 17681-17689.

[28] N. K. Allampally, M. J. Mayoral, S. Chansai, M. C. Lagunas, C. Hardacre, V. Stepanenko, R. Q. Albuquerque, G. Fernández, *Chem. Eur. J.* **2016**, *22*, 7810-7816.

[29] M. Kasha, H. R. Rawls, M. A. El-Bayoumi, *Pure Appl. Chem.* **1965**, *11*, 371–392.

[30] R. Q. Albuquerque, A. Timme, R. Kress, J. Senker, H.-W. Schmidt, *Chem. Eur. J.* **2013**, *19*, 1647-1657.

[31] M. Wegner, D. Dudenko, D. Sebastiani, A. R. A. Palmans, T. F. A. de Greef, R. Graf, H. W. Spiess, *Chem. Sci*. **2011**, *2*, 2040-2049.

Entry for the Table of Contents (Please choose one layout)

Layout 1:

FULL PAPER

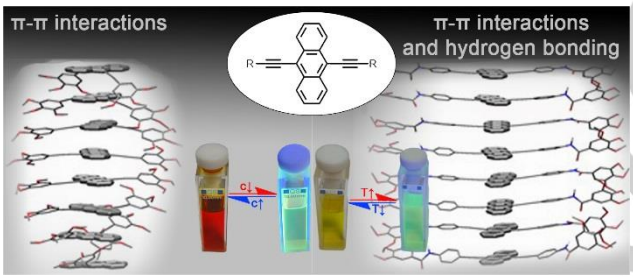

M. Lübtow, I. Helmers, Vladimir Stepanenko, R. Q. Albuquerque, T. B. Marder, G. Fernández **

Page No. – Page No.

Self-Assembly of 9,10-Bis(phenylethynyl)anthracene (BPEA) Derivatives: Influence of π–π and Hydrogen Bonding Interactions on Aggregate Morphology and Self-Assembly Mechanism